JACS Au
AN OPEN ACCESS JOURNAL OF THE AMERICAN CHEMICAL SOCIETY

pubs.acs.org/jacsau
Article

Harnessing a Pd_4 Water-Soluble Molecular Capsule as a Size-Selective Catalyst for Targeted Oxidation of Alkyl Aromatics

Valiyakath Abdul Rinshad, Medha Aggarwal, Jack K. Clegg, and Partha Sarathi Mukherjee*

Cite This: *JACS Au* 2024, 4, 3238−3247
Read Online

ACCESS | Metrics & More | Article Recommendations | Supporting Information

ABSTRACT: Molecular hosts with functional cavities can emulate enzymatic behavior through selective encapsulation of substrates, resulting in high chemo-, regio-, and stereoselective product formation. It is still challenging to synthesize enzyme-mimicking hosts that exhibit a narrow substrate scope that relies upon the recognition of substrates based on the molecular size. Herein, we introduce a Pd_4 self-assembled water-soluble molecular capsule $[M_4L_2]$ (**MC**) that was formed through the self-assembly of a ligand **L** (4′,4‴′-(1,4-phenylene)bis(1′,4′-dihydro-[4,2′:6′,4″-terpyridine]-3′,5′-dicarbonitrile)) with the acceptor *cis*-$[(en)Pd(NO_3)_2]$ [en = ethane-1,2-diamine] (**M**). The molecular capsule **MC** showed size-selective recognition towards xylene isomers. The redox property of **MC** was explored for efficient and selective oxidation of one of the alkyl groups of *m*-xylene and *p*-xylene to their corresponding toluic acids using molecular O_2 as an oxidant upon photoirradiation. Employing host−guest chemistry, we demonstrate the homogeneous catalysis of alkyl aromatics to the corresponding monocarboxylic acids in water under mild conditions. Despite homogeneous catalysis, the products were separated from the reaction mixtures by simple filtration/extraction, and the catalyst was reused. The larger analogues of the alkyl aromatics failed to bind within the **MC**'s hydrophobic cavity, resulting in a lower/negligible reaction outcome. The present study represents a facile approach for selective photo-oxidation of xylene isomers to their corresponding toluic acids in an aqueous medium under mild conditions.

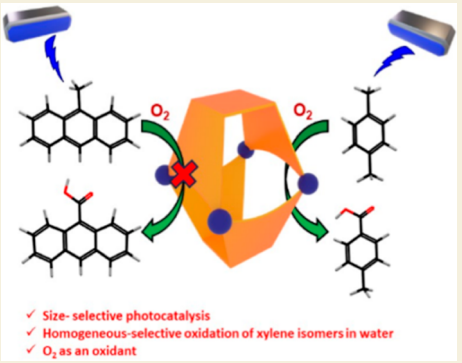

KEYWORDS: *self-assembly, host−guest, size-selective catalysis, xylene oxidation, coordination chemistry*

Enzymes facilitate various biochemical transformations with extraordinary catalytic power. The catalytic activity of enzymes arises from the targeted binding of substrate in the active sites, which are isolated microenvironments that stabilize transition states.[1−3] Several artificial molecular analogues of enzymes for catalysis have been developed.[4−9] Coordination-driven self-assembly is a technique for constructing various metal−organic architectures with defined geometry and cavities.[10−18] Beyond establishing diverse topologies, such functionalized molecular hosts have been employed for sensing,[19−21] stabilization of intermediates,[22−24] molecular recognition,[25−30] biological applications,[31−37] and catalysis.[38−46] Designing molecular architectures with specific cavities permits efficient catalysis, which differs significantly from the bulk reaction with unprecedented regio-, chemo-, and stereoselectivity.[47−52] Additionally, the close reactant proximity in cavities increases the reaction rates many times, allowing size-selective catalysis within a confined pocket.[53−57] Inspired by the substrate-specific catalysis mediated by cytochrome P450,[58−62] chemists have ventured into porous organic polymers,[63−65] metal−organic frameworks,[66−69] zeolites,[70−72] and covalent organic frameworks.[73−75] However, due to the solution processability, metal−organic cages have emerged as promising candidates for size-selective catalysis.[76,77] The precise control over the substrate in homogeneous catalysis opens avenues for designing reactions that would otherwise be challenging to achieve with traditional catalysts.

The oxidation of alkyl aromatics is an important class of organic reactions that generates valuable feedstocks for pesticides, perfumes, and fine chemical synthesis. Alkyl aromatics are primarily obtained as byproducts of the petrochemical industry.[78,79] The interest in oxidizing such volatile organic compounds to specific oxidized products is growing worldwide due to the conversion of hazardous molecules into valuable products.[80−82] Industrially, the carboxylic acid analogue is an important oxidized derivative of alkyl aromatics since it can be easily converted to ester, amides, acid chloride, alcohol, etc., in a single step.[83−87] The conventional oxidation of *m*-/*p*-xylenes usually requires a stoichiometric amount of permanganate or persulfate as the oxidant, and this process oxidizes both the methyl groups, leading to the formation of isophthalic acid/terephthalic acid.

Received: June 24, 2024
Revised: August 5, 2024
Accepted: August 6, 2024
Published: August 15, 2024

Selective oxidation of one of the methyl groups of xylenes to corresponding toluic acid is challenging, and transition metal complexes or metal oxides often achieve such oxidation at elevated temperatures.[88−92] Hence, selective oxidation of one of the methyl groups in xylene to corresponding toluic acid under mild conditions in an aqueous medium is challenging.[93,94] Often selective oxidation of xylenes to the toluic acids is obtained by heterogeneous catalysis due to the ease of separation.[95−97] Using water as a solvent would enable the advantages of easy separation as well as heterogeneous catalysis. Introducing a suitable water-soluble host capable of encapsulating the substrate could homogenize the reaction mixture. Furthermore, using molecular oxygen (O_2) as an oxidant will be ideal and align with the green chemistry principles. Another challenge in alkyl aromatics oxidation is activating the relatively unpolarized C−H bonds.[98−101] Light captured by the molecule could be an ideal energy source for C−H bond activation. The preorganization of a substrate within the cavity of the metal−organic cage can induce selectivity in photocatalytic reactions.[102] Recently, light-induced H atom abstraction of guest molecules through the preorganization of guests within the cavity, leading to the oxidation of alkyl aromatics to carbonyl compounds, has been reported by Dasgupta and co-workers.[103,104] In this case, the oxidation mechanism followed a radical pathway, and the cage can accept the electron from the guest molecules.

In this study, we report the design and synthesis of a new redox-active water-soluble molecular capsule [M_4L_2] (**MC**), which was prepared through self-assembly of a bent tetrapyridyl ligand (**L**) (4′,4‴′-(1,4-phenylene)bis(1′,4′-dihydro-[4,2′:6′,4″-terpyridine]-3′,5′-dicarbonitrile)) with a Pd(II) acceptor *cis*-[(en)Pd(NO_3)$_2$] (**M**) [en = ethane-1,2-diamine] (Scheme 1). A single-crystal X-ray diffraction study has established its molecular structure. Furthermore, the hydrophobic cavity of the **MC** was harnessed to encapsulate xylene isomers. Photoirradiation of the encapsulated *p*-/*m*-xylenes showed selective oxidation of one of the methyl groups to their corresponding toluic acids in an aqueous medium under ambient conditions. The photoirradiation of the encapsulated third isomer, *o*-xylene, resulted in the formation of *o*-toluic acid and lactone. Similarly, the photoirradiation of ethylbenzene (EB) in the presence of **MC** yielded exclusive formation of acetophenone. Such selective photo-oxidation of one of the methyl groups in xylene isomers at room temperature in the aqueous medium in a confined space is noteworthy as it demonstrates the potential for fine-tuned reactivity within the confined environment of **MC**; moreover, the narrow windows of the capsule played a significant role in inhibiting the encapsulation of larger alkyl aromatics and thereby impeding their oxidation, which manifests the use of **MC** in size-selective catalysis.

Scheme 1. Schematic Representation of Synthesis of MC Using L and M and the Selective Encapsulation and Oxidation of Xylene Isomers over Large Alkyl Aromatics

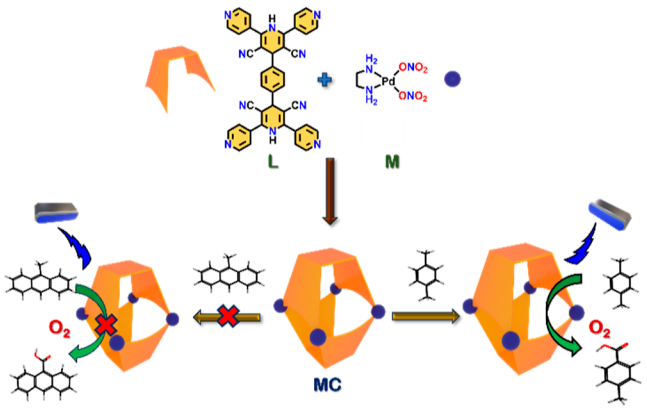

RESULTS AND DISCUSSION

The ligand (4′,4‴′-(1,4-phenylene)bis(1′,4′-dihydro-[4,2′:6′,4″-terpyridine]-3′,5′-dicarbonitrile)) (**L**) was prepared from the condensation reaction of *β*-amino-*β*-(pyrid-4-yl)-acrylonitrile with terephthaldehyde in acetic acid following the reported procedure.[105] **L** was characterized using NMR and ESI-MS analyses (Figures 1b and S1−S3). Previously, the ligand **L** was used to synthesize a supramolecular organic framework in the solid state due to the strong N−H···Npy hydrogen bond, which was used for CO_2 adsorption.[106,107] The self-assembly of **L** with the 90° acceptor *cis*-[(en)Pd(NO_3)$_2$] in a 1:2 molar ratio at 55 °C in DMSO for 12 h resulted in a clear red solution. ^{1}H NMR of this self-assembled product in DMSO-d_6 displayed six sharp peaks in the range of 4.8 to 10.2 ppm (Figure S4). The ^{1}H NMR in DMSO showed a significant downfield shift of the peaks compared to ligand **L** due to the metal−ligand coordination. The self-assembled product from the DMSO was precipitated by adding an excess amount of ethyl acetate, followed by washing with acetone and diethyl ether. The ^{1}H NMR spectrum of the product in D_2O showed three sharp peaks in the aromatic region ranging from 7.48 to 8.76 ppm (Figures 1a and S5). The ^{1}H-^{1}H COSY NMR spectrum showed the correlation of a and b protons, and the NOESY NMR spectrum showed the correlation between the acceptor and the ligand protons (Figures S6 and S7). Also, the ^{1}H DOSY NMR of the self-assembled product in water indicated the formation of a single architecture (Figures 1c and S8). The nature of the ^{1}H NMR spectrum of **MC** indicated the formation of a highly symmetric molecular architecture. Considering the ligand's folding nature, **L**'s self-assembly with the cis blocked 90° acceptor is expected to form a small M_4L_2 complex.

The ESI-MS analysis confirmed the composition of the self-assembled product. After the counterion exchange with the KPF_6, the ESI-MS mass spectrum showed major signals at m/z = 1412.0532, 893.0425, and 633.5446 corresponding to $[M_4L_2(PF_6)_6]^{2+}$ (calcd 1412.0598), $[M_4L_2(PF_6)_6]^{3+}$(calcd 893.0500), and $[M_4L_2(PF_6)_6]^{4+}$(calcd 633.5520) fragments, respectively (Figures 2a and S9). The NMR and ESI-MS suggested the formation of a Pd_4 molecular capsule (**MC**) by [4 + 2] self-assembly of the acceptor and donor. To confirm the conformation of the phenyl ring and the N···H unit, blocked-shaped orange crystals were successfully grown by the vapor diffusion of acetone into the aqueous **MC** and subjected to X-ray analysis. **MC** crystallizes in monoclinic *C*2/*m*.[108] In the crystal structure of the **MC**, the ligand adopts a concave geometry (the binding sites of the ligands are pointing toward one side), which is different from the stable folded confirmation of the free ligand (Figures 2b,c and S10). Two ligands are connected by four (en)Pd capping units to form a molecular capsule. The distance between alternate Pd centers is 17.1 Å, while the distance between the neighboring Pd atoms is around 12.5 Å. The central phenyl cores of the two ligands are aligned perpendicularly with a separation of 6.7 Å from

https://doi.org/10.1021/jacsau.4c00539
JACS Au 2024, 4, 3238−3247

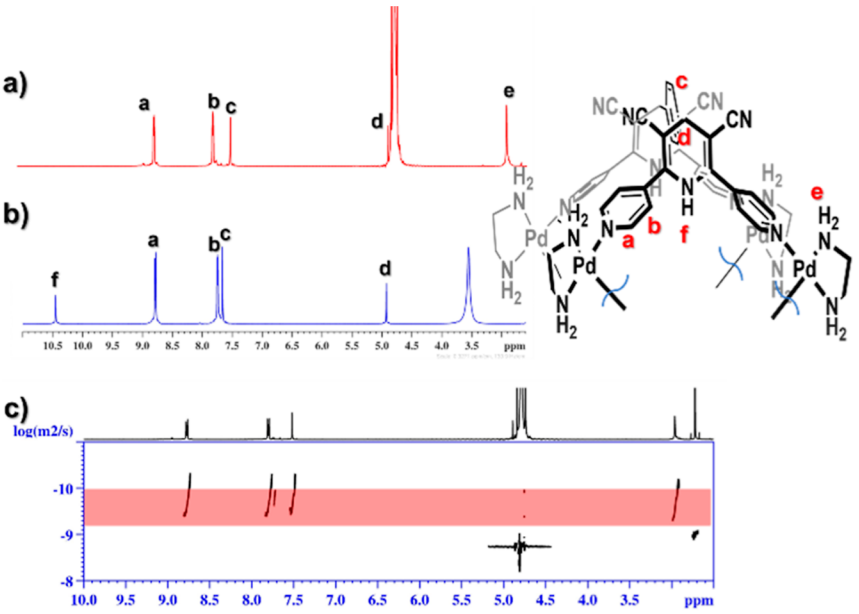

Figure 1. Stacked partial ^{1}H NMR spectra of the (a) cage **MC** in D_2O (400 MHz, 298 K), (b) ligand **L** in DMSO-d_6 (400 MHz, 298 K), and (c) ^{1}H DOSY NMR of **MC** in D_2O (400 MHz, 298 K).

each other. Also, the N···H moiety in the ligand is pointing outward to the cage. The occupied volume of the hydrophobic cavity of the **MC** was calculated to be 368 Å^3 using MoloVol (Figure 2d,e).[109]

We envisaged that the narrow cavity of **MC** could encapsulate molecules with a definite size and shape. The guest binding ability of **MC** was investigated by treating D_2O solution **MC** with excess amounts of PAHs such as naphthalene, pyrene, anthracene, and phenanthrene at room temperature and at elevated temperature. These guests showed no encapsulation in the **MC** cavity. It is potentially due to the ligand's non-aromatic nature, which restricts the encapsulation of PAHs due to the ineffective $\pi-\pi$ interactions. Hence, we turned our attention to encapsulating xylene isomers, which are smaller in size and can pass through the narrow hydrophobic cavity of **MC** with subsequent stabilization by C−H π interactions between the host and guest. The D_2O solution of the cage was treated separately with the four equivalent of the xylene isomers, *o*-xylene (OX), *m*-xylene (MX), *p*-xylene (MX), and EB and stirred for 2 h. The solutions were centrifugated and analyzed using NMR spectroscopy.

The ^{1}H NMR of the host−guest complex showed an upfield shift of the phenyl protons (c protons) and the nonaromatic protons (d protons), which suggests the binding of the guest molecules with **MC** (Figure 3). Additionally, the host−guest complexes were characterized by 2D NMR spectroscopy. The D_2O solution of **MC** was treated with an excess amount of guest molecules, and ^{1}H DOSY NMR spectra have been recorded (Figures S11−S14). The guest molecules that bind within the host showed a broad diffusion line in the ^{1}H DOSY NMR spectra, which is attributed to the fast equilibrium between the guest and host species with the host−guest adduct on the NMR time scale.

The host−guest stoichiometry and the association constant of each host−guest complex were calculated from the NMR titration experiments. NMR spectra were recorded after gradual addition of the MeOD solution of the OX to the D_2O solution of the **MC** (Figure 4). The ^{1}H NMR spectra showed the continuous shift of the host and guest peaks, which suggested a fast-exchange dynamic binding of OX within the cavity of **MC**. Similarly, other xylene isomers also exhibited dynamic binding with **MC**. To quantify the binding affinity of the xylene isomers within **MC**, the binding constants (K_a) were determined. The titration data obtained from the ^{1}H NMR experiments were fitted with a Hill function.[110] The obtained binding constants are 3.16×10^3 M^{-1} for OX, 2.05×10^3 M^{-1} for MX, 1.20×10^3 M^{-1} for PX, and 1.30×10^3 M^{-1} for EB (Table S2 and Figures S15−S21). These results further suggest that the OX binds relatively stronger than other isomers in the hydrophobic cavity of **MC**. Also, Job's plot between the molar fraction of **MC** against the change in the chemical shift of the host showed a maximum of 0.5, which suggests that one guest molecule is bound inside the cavity of **MC** (Figure S22).

To better understand the orientation of the guest molecules within **MC**, the structures of the OX⊂**MC**, PX⊂**MC**, MX⊂**MC**, and EB⊂**MC** were optimized using the PM6 Model.[111] The optimized structures showed a perfect fitting of the xylene isomers within the cavity of **MC**. For example, the optimized structure of the EB⊂**MC** showed C−H -π interaction between EB and the host. Similarly, the OX, PX, and MX fit perfectly within the hydrophobic cavity of **MC** (Figure S23).

The successful encapsulation of xylene isomers within the cavity of the redox-active host (**MC**) prompted us to activate the weakly polarized C−H bond of alkyl aromatics. Encapsulation of organic substrates in molecular cages is expected to promote polarization of C−H bonds for oxidation.[112,113] Selective oxidation of one of the alkyl groups of *m*-/*p*-xylene is always challenging. Conventional oxidation methods need high temperature and strong oxidizing agents like alkaline $KMnO_4$ that oxidize both the alkyl groups to yield corresponding dicarboxylic acids. Selective oxidation of one of the methyl groups generally requires special catalysts. We anticipated that a water-soluble redox active cage might facilitate such an oxidation reaction by reducing the activation

https://doi.org/10.1021/jacsau.4c00539
JACS Au 2024, 4, 3238−3247

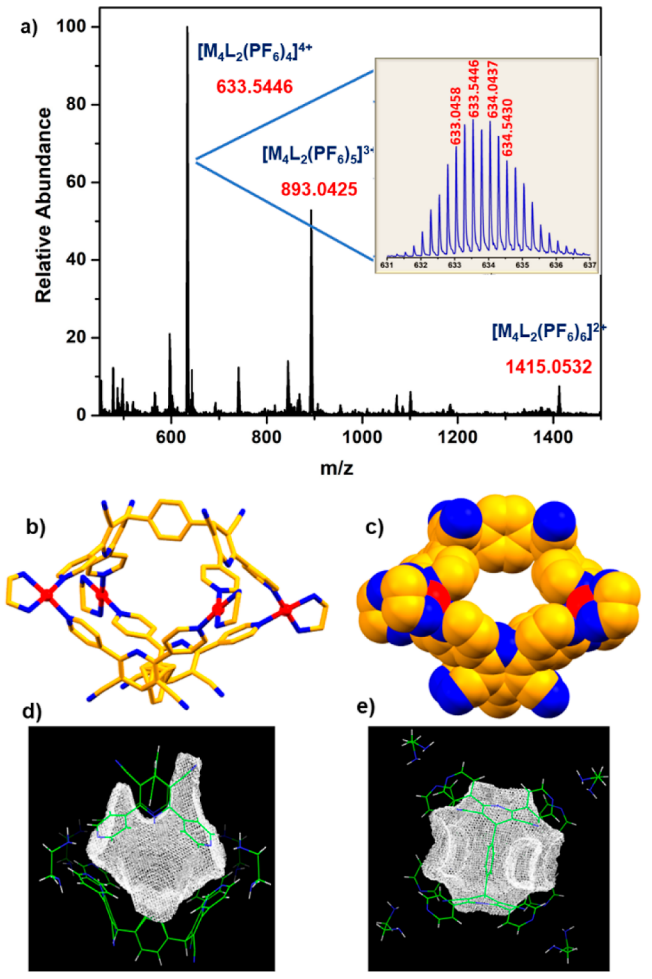

Figure 2. (a) ESI-MS spectrum of the PF_6^- analogue of **MC** in acetonitrile. Experimental isotopic distribution pattern of the $[\mathbf{MC}(PF_6)_4]^{4+}$ fragment (inset). (b) Capped stick model of the single crystal XRD structure (CCDC no. 2268668) of **MC** (color codes: yellow = carbon, blue = nitrogen, and red = palladium; the anions and solvent molecules were omitted for clarity). (c) Space-filled model of **MC**. (d) Side-view of the cavity volume (shown as white mesh) of **MC**. (e) Top side view of the cavity of **MC**.

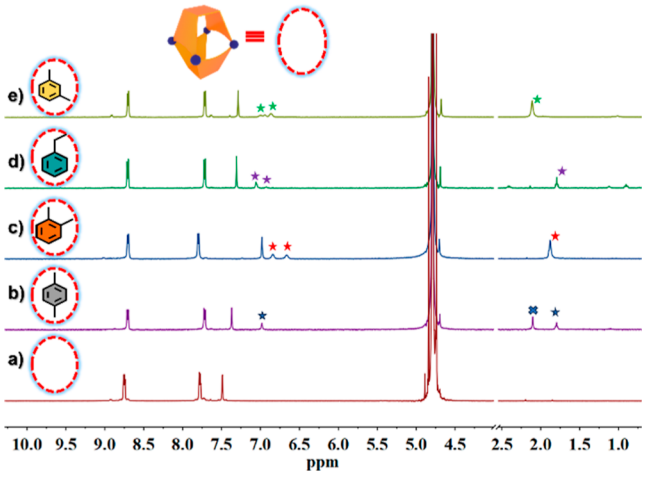

Figure 3. Partial ^{1}H NMR stack plot of (a) **MC**, (b) PX⊂**MC**, (c) OX⊂**MC**, (d) EB⊂**MC**, and (e) MX⊂**MC** (400 MHz, 298 K, D_2O/MeOD (4:1)). The stars represent the guest peaks. The cross denotes the acetone solvent impurity.

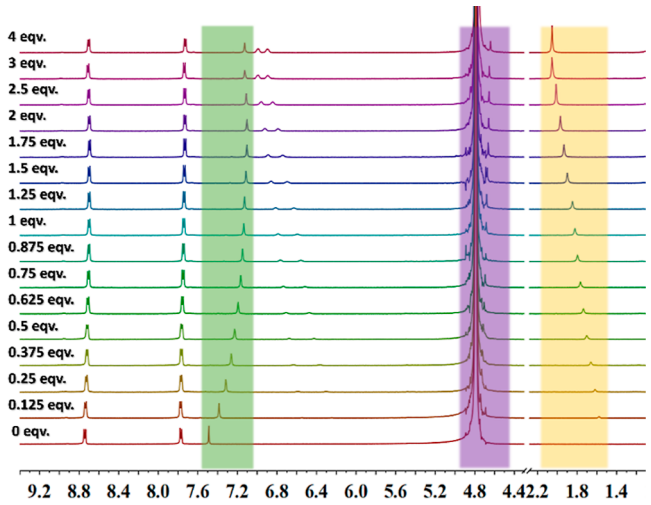

Figure 4. ^{1}H NMR titration of **MC** with the gradual addition of *o*-xylene (OX). The changes in the chemical shifts of the c and d protons of the host are highlighted by green and violet boxes, respectively. Change in the chemical shift of the methyl protons of the OX is highlighted in the yellow box.

energy in a confined space and thus lead to the formation of oxidized products under room temperature with selective oxidation of one of the methyl groups. UV−vis spectra of the **MC** and xylene/EB encapsulated complexes have been recorded. The host **MC** showed an absorption band at around 392 nm (Figure S24). Hence, a 390 nm blue LED (40 W) was utilized for irradiation. Cyclic voltammetry studies of **MC** showed a sharp reduction potential at −0.24 V and a broad oxidation potential at 0.04 V (Figure S25). In view of that, EB was chosen as the model compound (Table 1), and the

Table 1. Optimization of the Photo-oxidation of Ethyl Benzene[a]

entry	catalyst	condition	time (h)	light	conversion[a] (selectivity)
1	**MC** (5 mol %)	O_2	12	ON	97 (96)
2	**MC** (1 mol %)	O_2	12	ON	40.3 (92)
3	**MC** (5 mol %)	O_2	12	OFF	7.4 (78)
4	**M** (5 mol %)	O_2	12	ON	3 (99)
5	**L** (5 mol %)	O_2	12	ON	2.4 (99)
6	nil	O_2	12	ON	2 (53)
7	**MC** (5 mol %)	N_2	12	ON	6 (85)
7	**MC** (5 mol %), TMP	O_2	12	ON	85 (87)
8	**MC** (5 mol %), BQ	O_2	12	ON	48 (80)

[a]The conversion has been calculated from ^{1}H NMR spectroscopy.

EB⊂**MC** was irradiated under blue LEDs for 12 h at room temperature in the presence of O_2 (Figure S26). The product was extracted with ethyl acetate and characterized by NMR spectroscopy after the solvent was evaporated under reduced pressure. The ^{1}H NMR spectrum confirmed that acetophenone was selectively formed with 97% conversion and 96% selectivity. The control experiments with the ligand **L** and the metal acceptor **M** showed only 2.4 and 3% conversions, respectively (Figure S27), under the same reaction conditions. Similarly, the reaction under dark conditions in the presence of **MC** resulted in a 7.4% conversion of EB to acetophenone. The

https://doi.org/10.1021/jacsau.4c00539
JACS Au 2024, 4, 3238−3247

reaction was optimized by loading 5 mol % **MC**. The control experiments showed that **MC**, blue LED light, and O_2 are indispensable parts of the photocatalytic reaction. Moreover, experiments have been carried out with benzoquinone (BQ) and 2,2,6,6-tetramethylpiperidine (TMP) to elucidate the mechanism of photocatalysis. The reaction with BQ, a well-known radical quencher, showed an evident drop in the conversion to 48%, while the reaction with TMP (singlet oxygen quencher) showed a conversion of around 85%. Furthermore, the photo-oxidation of 4-tert butyl toluene in the presence of TEMPO resulted in the formation of a TEMPO adduct with the radical (Figure S28). The above control experiments suggest that the reaction undergoes through the radical pathway. Furthermore, we examined the recyclability of **MC** up to three cycles in the photo-oxidation. It showed **MC**'s negligible loss of activity.

The unusual oxidation of the relatively nonpolarized C−H bonds of alkyl aromatics to the corresponding acids prompted us to investigate the underlying mechanism of the reaction. The structure of the host−guest complex (PX⊂**MC**) and the in situ generated radical of PX within **MC** (PẊ⊂MC) were optimized semi-empirically using the PM6 model. The optimized PX⊂**MC** structure revealed the stabilization of the guest molecule within the cavity through robust C−H··· π interactions (3.01 Å) between PX and the ligand core form a perfect fit within the void of **MC**. Furthermore, the proximity of one of the methyl groups of PX and the C−H bond of the central phenyl core at 2.7 Å indicated the effective binding of the guest molecule. Conversely, optimized PẊ⊂**MC** showed that the radical species was centered around one of the narrow windows of **MC** (Figure 5). Such preorganization indicates

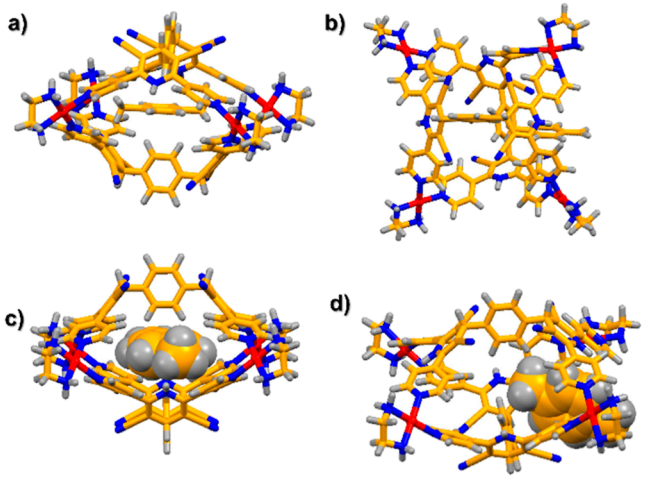

Figure 5. (a) Capped stick model of the optimized structure of PX⊂**MC** (color codes: yellow = carbon, blue = nitrogen, gray = hydrogen, and red = palladium). (b) Optimized structure of the PX radical with **MC** (PẊ⊂**MC**). (c) Optimized structure of PX⊂**MC**. (d) Optimized structure of PẊ⊂**MC**.

that the radicals generated within the cavity could undergo a facile reaction with the molecular oxygen in the solution. Also, the PẊ radical has been stabilized within the cavity with a weak C−H···π interaction (3.65 Å) with the pyridine core of the ligand.

Further, the generation of radical species within the molecular capsule upon irradiation was determined by ESR analysis. The PX⊂**MC** solution was frozen using liquid nitrogen, and ESR was recorded before and after irradiation. Upon irradiation, two broad peaks corresponding to the generated radical are shown (Figure S30). The results showed that radical generation and oxidation are simultaneous processes.

The hydrophobic cavity of the **MC** was expected to assist the release of the photo-oxidized product from the host. Additionally, the facile displacement of the carboxylic acids from the cavity can be accounted for by the fact that the carboxylic group has a higher free energy of solvation in water compared with that of PX. This insight supports the fact that the reaction proceeds favorably through the radical pathway within the host−guest complex, which renders the reaction catalytic in nature, facilitated by easy product elimination from the cavity of **MC**. Moreover, we turned our attention to examining the stabilization of the radical intermediates within the cavity of **MC** (Figure 6 and Table S4). Also, semiempirical

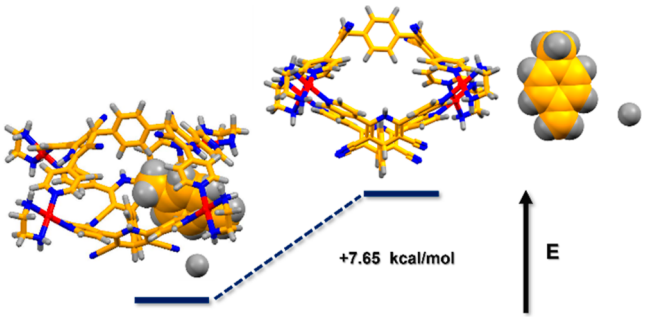

Figure 6. Calculated structures (PM6) and relative energies of PẊ⊂**MC** (left) and MC and PẊ radical (right). (Color codes: to rank the relative energies of the host−guest complex (PẊ⊂**MC**) yellow = carbon, blue = nitrogen, gray = hydrogen, and red = palladium).

energy calculations (PM6) were performed to calculate the energy of the host−guest radical adduct. These calculations suggested that the *p*-xylene radical (PẊ) within the capsule was thermodynamically favored by −7.65 kcal/mol compared to the free *p*-xylene radical (PẊ). Based on the experimental evidence and previous literature reports, a plausible reaction mechanism has been proposed in Figure S29 (Supporting Information). The other isomers of xylene and derivatives were also explored to generalize the photocatalysis (Table 2). The reaction of MX and PX resulted in the formation of monocarboxylic acid along with a minor amount of aldehyde (Figures S35−S37). The control experiments of photo-oxidation of *p*-xylene with **M** and **L** were performed. The reaction with **M** did not result in acid formation, and the reaction with **L** showed negligible acid formation (2% yield was observed). It further suggests that the oxidation of *p*-xylene to the corresponding acid is possible only in the presence of the **MC**.

Moreover, the thermodynamic feasibility of electron transfer between the PX and **MC** was analyzed using the Rehm−Weller equation (see Supporting Information).[114,115] The oxidation and reduction potentials of *p*-xylene and **MC** were used to calculate the free energy change in the electron transfer. The ΔG was found to be negative, suggesting that such electron transfer is feasible thermodynamically.

Photooxidation was further explored using 4-*tert*-butyl toluene, which also showed the selective formation of monocarboxylic acid (Figures S33 and S34). To confirm the

https://doi.org/10.1021/jacsau.4c00539
JACS Au 2024, 4, 3238−3247

Table 2. Photocatalytic Oxidation of Alkyl Aromatics

Entry	Substrate	Condition	Time	Products Conversion[a]		
1		**MC**(5 mol%) O_2, 390 nm	16 h	 (91%)	 (9%)	
2		**MC**(5 mol%) O_2, 390 nm	16 h	 (87%)	 (13%)	
3		**MC**(5 mol%) O_2, 390 nm	16 h	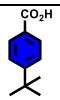 (98%)		
4		**MC**(5 mol%) O_2, 390 nm	16h	 (96%)		
5		**MC**(5 mol%) O_2, 390 nm	16h	 (25%)	 (26%)	 (38%)
6		**MC**(5 mol%) O_2, 390 nm	12h	 (97%)		
7		**MC**(5 mol%) O_2, 390 nm	16h	 n.d[b]		
8		**MC**(5 mol%) O_2, 390 nm	16h	 n.d		

[a]Determined by ^{1}H NMR spectroscopy. [b]n.d. = not detected.

stepwise oxidation, 4-tolualdehyde was irradiated in the presence of **MC** (Figure S38). After extraction with chloroform, the ^{1}H NMR spectrum showed the exclusive formation of the acid. Surprisingly, in the reaction of the OX under the optimized reaction conditions, the monocarboxylic acid undergoes further oxidation with the proximal methyl group to form the lactone, which has been detected in the GC−MS analysis (Figures S40 and S41).

To check if the encapsulation of the substrates inside **MC** promoted the reaction and if the substrate's size has any role in such oxidation in the presence of **MC**, higher analogues of alkyl aromatics such as mesitylene, durene, 1-methylnaphthalene, 9-methyl anthracene, and 6-methyl coumarin were irradiated in the presence of **MC**. No oxidation was noticed in these cases. Such large guest molecules did not show any binding with the **MC**. Titration of 9-methyl anthracene with the D_2O solution of **MC** did not show any shift of the guest or host protons due to the mismatch of the window size of **MC** with the size of the guests (Figure S31). A similar observation was also noticed in the presence of the other large alkyl aromatics mentioned above. To validate the size-selective behavior of **MC**, competitive photo-oxidation of 9-methyl anthracene and EB was carried out in the presence of **MC**. The reaction mixture was extracted with $CDCl_3$, and the ^{1}H NMR spectrum showed the exclusive oxidation of EB. The reaction of higher alkyl aromatics analogues did not yield any product under the same reaction condition in the presence of 5 mol % **MC**, even under prolonged irradiation (48 h) of light. It demonstrates that the encapsulation of the substrates in the cavity of **MC** plays a significant role in the photo-oxidation through the preorganization of guest molecules, followed by the stabilization of radicals formed during the irradiation.

CONCLUSIONS

In conclusion, this work describes the design and synthesis of a new water-soluble molecular capsule **MC** that was obtained by the self-assembly of a redox-active tetrapyridyl donor in combination with a *cis*-Pd(II) acceptor. The single crystal X-ray diffraction study of **MC** revealed the formation of a rigid nanocavity, which has been explored for the encapsulation of xylene isomers. The xylene isomers showed a dynamic binding within the cage, and Job's plot revealed the formation of 1:1 host−guest complexes with the xylene isomers. Further, the photooxidase-mimicking property of **MC** was explored by the effective photo-oxidation of the sp^3 C−H bond present in the alkyl aromatics. While conventional oxidation of *m*-xylene/*p*-xylene using oxidants like permanganate or dichromate generally oxidizes both the alkyl groups, leading to the formation of isophthalic/terephthalic acids. The selective oxidation of one of the two methyl groups in xylene needs transition metal-based special catalysts and high temperature (∼120 °C), even though such approach gives a mixture of products. Encapsulated xylenes (*meta*- and *para*-) within the **MC** showed facile and selective photo-oxidation of one of the methyl groups to their corresponding toluic acids at ambient temperature in the aqueous medium. Encapsulated EB in the confined cavity of **MC** upon photo-oxidation yielded acetophenone selectively without any trace of the corresponding acid. Mechanistic studies suggest that the reaction proceeds through the radical pathway. The effective stabilization of the radical generated using photoirradiation in the confined cavity of **MC** plays a crucial role in the facile and selective photo-oxidation of one of the alkyl groups in *m*-/*p*-xylene. Further research established that such oxidation is encapsulation-promoted and size-selective. Larger alkyl aromatics did not show any encapsulation; thus, they were inactive in such photooxidation under the same reaction conditions in the presence of **MC**. Our present study demonstrates a facile approach of selective photooxidation of sp^3 C−H bonds of one of the alkyl groups of xylene isomers under ambient conditions in an aqueous medium in a molecular capsule's (**MC**) confined space.

METHODS

All chemicals and solvents were commercially available and used directly without further purification. The ^{1}H NMR, ^{13}C NMR, DOSY, 2D ^{1}H−^{1}H COSY, and ^{1}H−^{1}H NOESY were recorded using Bruker 400 and 500 MHz instruments in deuterated solvents. The chemical shifts in the spectra are reported relative to TMS (0.0 ppm) or proton resonance resulting from the incomplete deuteration of DMSO (2.50 ppm), MeOD (3.31 ppm), $CDCl_3$ (7.26 ppm), and D_2O (4.79 ppm). Electrospray ionization mass spectrometric (ESI-MS) analyses were carried out on an Agilent 6538 Ultra-High-Definition (UHD) Accurate Mass Q-TOF spectrometer in standard spectroscopic grade solvents. UV−vis spectra were recorded using a PerkinElmer LAMBDA-750 spectrophotometer. All theoretical calculations were performed using the Gaussian 09 package. The host−guest complexes

https://doi.org/10.1021/jacsau.4c00539
JACS Au 2024, 4, 3238−3247

PX⊂**MC**, OX⊂**MC**, EB⊂**MC**, and MX⊂**MC** were optimized using the PM6 semiempirical method. No symmetry constraints were used during the optimization.

■ ASSOCIATED CONTENT

Supporting Information

The Supporting Information is available free of charge at https://pubs.acs.org/doi/10.1021/jacsau.4c00539.

Additional NMR, ESI-MS spectra, experimental details, and optimized structure of the host−guest complex (PDF)

X-ray crystallographic data for host **MC** (CIF)

■ AUTHOR INFORMATION

Corresponding Author

Partha Sarathi Mukherjee − *Department of Inorganic and Physical Chemistry, Indian Institute of Science, Bangalore 560012, India;* orcid.org/0000-0001-6891-6697; Email: psm@iisc.ac.in

Authors

Valiyakath Abdul Rinshad − *Department of Inorganic and Physical Chemistry, Indian Institute of Science, Bangalore 560012, India*

Medha Aggarwal − *Department of Inorganic and Physical Chemistry, Indian Institute of Science, Bangalore 560012, India*

Jack K. Clegg − *School of Chemistry and Molecular Biosciences, The University of Queensland, St. Lucia, Queensland 4072, Australia;* orcid.org/0000-0002-7140-5596

Complete contact information is available at: https://pubs.acs.org/10.1021/jacsau.4c00539

Author Contributions

V.A.R carried out the experimental works. V.A.R. and M.A. analyzed the experimental data. J.K.C. contributed to X-ray structure determination. P.S.M. supervised the project. The manuscript was written through contributions of all the authors. All authors have given approval to the final version of the manuscript. CRediT: **Valiyakath Abdul Rinshad** data curation, formal analysis, investigation, writing-original draft; **Medha Aggarwal** data curation, formal analysis, investigation, methodology, writing-original draft.

Notes

The authors declare no competing financial interest.

■ ACKNOWLEDGMENTS

P.S.M. thanks SERB-India for research grant and the J. C. Bose fellowship. V.A.R. is thankful to the Ministry of Education (India) for PMRF fellowship. The authors are thankful to Prof. Mrinmoy De for the photoirradiation setup and Dr. M. Venkateswarulu for the fruitful discussions. Authors are also thankful to Dr. Garima Jindal for fruitful discussion on the optimization of the radical in cage.

■ REFERENCES

(1) Wolfenden, R.; Snider, M. J. The depth of chemical time and the power of enzymes as catalysts. *Acc. Chem. Res.* **2001**, *34*, 938−945.

(2) Wolfenden, R. Transition state analogues for enzyme catalysis. *Nature* **1969**, *223*, 704−705.

(3) Demetrius, L. Role of enzyme−substrate flexibility in catalytic activity: an evolutionary perspective. *J. Theor. Biol.* **1998**, *194*, 175−194.

(4) Chen, Y.; Yang, Y.; Orr, A. A.; Makam, P.; Redko, B.; Haimov, E.; Wang, Y.; Shimon, L. J.; Rencus-Lazar, S.; Ju, M.; et al. Self-assembled peptide nano-superstructure towards enzyme mimicking hydrolysis. *Angew. Chem., Int. Ed.* **2021**, *60*, 17164−17170.

(5) Lyu, Y.; Scrimin, P. Mimicking Enzymes: The quest for powerful catalysts from simple molecules to nanozymes. *ACS Catal.* **2021**, *11*, 11501−11509.

(6) Li, W.-L.; Head-Gordon, T. Catalytic principles from natural enzymes and translational design strategies for synthetic catalysts. *ACS Cent. Sci.* **2021**, *7*, 72−80.

(7) Shi, Y.; Zhang, X.; Liu, H.; Han, J.; Yang, Z.; Gu, L.; Tang, Z. Metalation of catechol-functionalized defective covalent organic frameworks for lewis acid catalysis. *Small* **2020**, *16*, 2001998.

(8) Nothling, M. D.; Xiao, Z.; Bhaskaran, A.; Blyth, M. T.; Bennett, C. W.; Coote, M. L.; Connal, L. A. Synthetic catalysts inspired by hydrolytic enzymes. *ACS Catal.* **2019**, *9*, 168−187.

(9) Raynal, M.; Ballester, P.; Vidal-Ferran, A.; van Leeuwen, P. W. Supramolecular catalysis. Part 2: artificial enzyme mimics. *Chem. Soc. Rev.* **2014**, *43*, 1734−1787.

(10) Pullen, S.; Tessarolo, J.; Clever, G. H. Increasing structural and functional complexity in self-assembled coordination cages. *Chem. Sci.* **2021**, *12*, 7269−7293.

(11) Northrop, B. H.; Zheng, Y.-R.; Chi, K.-W.; Stang, P. J. Self-organization in coordination-driven self-assembly. *Acc. Chem. Res.* **2009**, *42*, 1554−1563.

(12) Chakrabarty, R.; Mukherjee, P. S.; Stang, P. J. Supramolecular coordination: self-assembly of finite two-and three-dimensional ensembles. *Chem. Rev.* **2011**, *111*, 6810−6918.

(13) Han, M.; Engelhard, D. M.; Clever, G. H. Self-assembled coordination cages based on banana-shaped ligands. *Chem. Soc. Rev.* **2014**, *43*, 1848−1860.

(14) Smulders, M. M.; Riddell, I. A.; Browne, C.; Nitschke, J. R. Building on architectural principles for three-dimensional metallosupramolecular construction. *Chem. Soc. Rev.* **2013**, *42*, 1728−1754.

(15) Nitschke, J. R. Construction, substitution, and sorting of metallo-organic structures via subcomponent self-assembly. *Acc. Chem. Res.* **2007**, *40*, 103−112.

(16) Stefankiewicz, A. R.; Sambrook, M. R.; Sanders, J. K. Template-directed synthesis of multi-component organic cages in water. *Chem. Sci.* **2012**, *3*, 2326−2329.

(17) Zhang, H. N.; Jin, G. X. Controllable Topological Transformations of 818 Molecular Metalla-knots by Oxidation of Thiazole-Based Ligands. *Angew. Chem., Int. Ed.* **2023**, *62*, No. e202313605.

(18) Xu, L.; Wang, Y.-X.; Chen, L.-J.; Yang, H.-B. Construction of multiferrocenyl metallacycles and metallacages via coordination-driven self-assembly: from structure to functions. *Chem. Soc. Rev.* **2015**, *44*, 2148−2167.

(19) Liu, C.-L.; Zhou, L.-P.; Tripathy, D.; Sun, Q.-F. Self-assembly of stable luminescent lanthanide supramolecular M 4 L 6 cages with sensing properties toward nitroaromatics. *Chem. Commun.* **2017**, *53*, 2459−2462.

(20) Shanmugaraju, S.; Mukherjee, P. S. π-Electron rich small molecule sensors for the recognition of nitroaromatics. *Chem. Commun.* **2015**, *51*, 16014−16032.

(21) Lakshmi, P. R.; Mohan, B.; Kang, P.; Nanjan, P.; Shanmugaraju, S. Recent advances in fluorescence chemosensors for ammonia sensing in the solution and vapor phases. *Chem. Commun.* **2023**, *59*, 1728−1743.

(22) Brumaghim, J. L.; Michels, M.; Pagliero, D.; Raymond, K. N. Encapsulation and stabilization of reactive aromatic diazonium ions and the tropylium ion within a supramolecular host. *Eur. J. Org Chem.* **2004**, *2004*, 5115−5118.

(23) Dong, V. M.; Fiedler, D.; Carl, B.; Bergman, R. G.; Raymond, K. N. Molecular recognition, and stabilization of iminium ions in water. *J. Am. Chem. Soc.* **2006**, *128*, 14464−14465.

(24) Nguyen, Q. N. N.; Xia, K. T.; Zhang, Y.; Chen, N.; Morimoto, M.; Pei, X.; Ha, Y.; Guo, J.; Yang, W.; Wang, L.-P.; et al. Source of Rate Acceleration for Carbocation Cyclization in Biomimetic Supramolecular Cages. *J. Am. Chem. Soc.* **2022**, *144*, 11413−11424.
(25) Howlader, P.; Mondal, B.; Purba, P. C.; Zangrando, E.; Mukherjee, P. S. Self-assembled Pd (II) barrels as containers for transient merocyanine form and reverse thermochromism of spiropyran. *J. Am. Chem. Soc.* **2018**, *140*, 7952−7960.
(26) Niki, K.; Tsutsui, T.; Yamashina, M.; Akita, M.; Yoshizawa, M. Recognition and stabilization of unsaturated fatty acids by a polyaromatic receptor. *Angew. Chem., Int. Ed.* **2020**, *59*, 10575−10578.
(27) Preston, D.; Sutton, J. J.; Gordon, K. C.; Crowley, J. D. A Nona-nuclear Heterometallic Pd3Pt6 "Donut" -Shaped Cage: Molecular Recognition and Photocatalysis. *Angew. Chem., Int. Ed.* **2018**, *57*, 8659−8663.
(28) Chen, G.-H.; He, Y.-P.; Yu, Y.; Li, Q.-H.; Zhang, J. Homochiral design of titanium-organic cage for circularly polarized luminescence-based molecular detection. *Sci. China: Chem.* **2023**, *66*, 2558−2562.
(29) Xie, S.-M.; Fu, N.; Li, L.; Yuan, B.-Y.; Zhang, J.-H.; Li, Y.-X.; Yuan, L.-M. Homochiral metal−organic cage for gas chromatographic separations. *Anal. Chem.* **2018**, *90*, 9182−9188.
(30) Tamura, Y.; Takezawa, H.; Fujita, M. A double-walled knotted cage for guest-adaptive molecular recognition. *J. Am. Chem. Soc.* **2020**, *142*, 5504−5508.
(31) Feng, Q.; Li, R.; Gao, T.; Chu, D.; Zhang, M. Emissive metallacages for biomedical applications. *Sci. China: Chem.* **2023**, *66*, 2447−2459.
(32) Sokolow, G. E.; Crawley, M. R.; Morphet, D. R.; Asik, D.; Spernyak, J. A.; McGray, A. J. R.; Cook, T. R.; Morrow, J. R. Metal−Organic Polyhedron with Four Fe (III) Centers Producing Enhanced T1Magnetic Resonance Imaging Contrast in Tumors. *Inorg. Chem.* **2022**, *61*, 2603−2611.
(33) Zhao, X.; Liu, J.; Fan, J.; Chao, H.; Peng, X. Recent progress in photosensitizers for overcoming the challenges of photodynamic therapy: from molecular design to application. *Chem. Soc. Rev.* **2021**, *50*, 4185−4219.
(34) Ahmad, N.; Younus, H. A.; Chughtai, A. H.; Verpoort, F. Metal−organic molecular cages: applications of biochemical implications. *Chem. Soc. Rev.* **2015**, *44*, 9−25.
(35) Judge, N.; Wang, L.; Ho, Y. Y. L.; Wang, Y. Molecular engineering of metal-organic cycles/cages for drug delivery. *Macromol. Res.* **2018**, *26*, 1074−1084.
(36) Hu, G.; Liu, Q.; Zhou, Y.; Yan, W.; Sun, Y.; Peng, S.; Zhao, C.; Zhou, X.; Deng, H. Extremely Large 3D Cages in Metal−Organic Frameworks for Nucleic Acid Extraction. *J. Am. Chem. Soc.* **2023**, *145*, 13181−13194.
(37) Abdul Rinshad, V.; Sahoo, J.; Venkateswarulu, M.; Hickey, N.; De, M.; Sarathi Mukherjee, P. Solvent Induced Conversion of a Self-Assembled Gyrobifastigium to a Barrel and Encapsulation of Zinc-Phthalocyanine within the Barrel for Enhanced Photodynamic Therapy. *Angew. Chem., Int. Ed.* **2023**, *62*, No. e202218226.
(38) Otte, M.; Kuijpers, P. F.; Troeppner, O.; Ivanović-Burmazović, I.; Reek, J. N.; de Bruin, B. Encapsulation of Metalloporphyrins in a Self-Assembled Cubic M8L6 Cage: A New Molecular Flask for Cobalt−Porphyrin-Catalysed Radical-Type Reactions. *Chem.—Eur. J.* **2013**, *19*, 10170−10178.
(39) Das, P.; Kumar, A.; Howlader, P.; Mukherjee, P. S. A Self-Assembled Trigonal Prismatic Molecular Vessel for Catalytic Dehydration Reactions in Water. *Chem.—Eur. J.* **2017**, *23*, 12565−12574.
(40) Chen, S.; Li, K.; Zhao, F.; Zhang, L.; Pan, M.; Fan, Y.-Z.; Guo, J.; Shi, J.; Su, C.-Y. A metal-organic cage incorporating multiple light harvesting and catalytic centres for photochemical hydrogen production. *Nat. Commun.* **2016**, *7*, 13169.
(41) Chu, D.; Gong, W.; Jiang, H.; Tang, X.; Cui, Y.; Liu, Y. Boosting enantioselectivity of chiral molecular catalysts with supramolecular metal−organic cages. *CCS Chem.* **2022**, *4*, 1180−1189.
(42) Zhu, F.-F.; Chen, L.-J.; Chen, S.; Wu, G.-Y.; Jiang, W.-L.; Shen, J.-C.; Qin, Y.; Xu, L.; Yang, H.-B. Confinement self-assembly of metal-organic cages within mesoporous carbon for one-pot sequential reactions. *Chem* **2020**, *6*, 2395−2406.
(43) Chen, S.; Chen, L.-J. Metal−Organic Cages: Applications in Organic Reactions. *Chemistry* **2022**, *4*, 494−519.
(44) Ham, R.; Nielsen, C. J.; Pullen, S.; Reek, J. N. Supramolecular coordination cages for artificial photosynthesis and synthetic photocatalysis. *Chem. Rev.* **2023**, *123*, 5225−5261.
(45) Jongkind, L. J.; Caumes, X.; Hartendorp, A. P.; Reek, J. N. Ligand template strategies for catalyst encapsulation. *Acc. Chem. Res.* **2018**, *51*, 2115−2128.
(46) Leenders, S. H.; Gramage-Doria, R.; de Bruin, B.; Reek, J. N. Transition metal catalysis in confined spaces. *Chem. Soc. Rev.* **2015**, *44*, 433−448.
(47) Genov, G. R.; Takezawa, H.; Hayakawa, H.; Fujita, M. Tetradehydro-Diels−Alder Reactions of Flexible Arylalkynes via Folding Inside a Molecular Cage. *J. Am. Chem. Soc.* **2023**, *145*, 17013−17017.
(48) Kusukawa, T.; Nakai, T.; Okano, T.; Fujita, M. Remarkable acceleration of Diels−Alder reactions in a self-assembled coordination cage. *Chem. Lett.* **2003**, *32*, 284−285.
(49) Yoshizawa, M.; Tamura, M.; Fujita, M. Diels-Alder in aqueous molecular hosts: unusual regioselectivity and efficient catalysis. *Science* **2006**, *312*, 251−254.
(50) Lu, Z.; Ronson, T. K.; Heard, A. W.; Feldmann, S.; Vanthuyne, N.; Martinez, A.; Nitschke, J. R. Enantioselectivefullerene functionalization through stereochemical information transfer from a self-assembled cage. *Nat. Chem.* **2023**, *15*, 405−412.
(51) Li, X.; Wu, J.; He, C.; Meng, Q.; Duan, C. Asymmetric catalysis within the chiral confined space of metal−organic architectures. *Small* **2019**, *15*, 1804770.
(52) Guo, J.; Xu, Y. W.; Li, K.; Xiao, L. M.; Chen, S.; Wu, K.; Chen, X. D.; Fan, Y. Z.; Liu, J. M.; Su, C. Y. Regio-and enantioselective photodimerization within the confined space of a homochiral ruthenium/palladium heterometallic coordination cage. *Angew. Chem., Int. Ed.* **2017**, *56*, 3852−3856.
(53) Otte, M. Size-selective molecular flasks. *ACS Catal.* **2016**, *6*, 6491−6510.
(54) Merlau, M. L.; del Pilar Mejia, M.; Nguyen, S. T.; Hupp, J. T. Artificial enzymes formed through directed assembly of molecular square encapsulated epoxidation catalysts. *Angew. Chem., Int. Ed.* **2001**, *40*, 4239−4242.
(55) Lee, S. J.; Cho, S.-H.; Mulfort, K. L.; Tiede, D. M.; Hupp, J. T.; Nguyen, S. T. Cavity-tailored, self-sorting supramolecular catalytic boxes for selective oxidation. *J. Am. Chem. Soc.* **2008**, *130*, 16828−16829.
(56) Leung, D. H.; Fiedler, D.; Bergman, R. G.; Raymond, K. N. Selective C— H Bond Activation by a Supramolecular Host−Guest Assembly. *Angew. Chem., Int. Ed.* **2004**, *43*, 963−966.
(57) Jiao, Y.; Wang, J.; Wu, P.; Zhao, L.; He, C.; Zhang, J.; Duan, C. Cerium-Based M4L4 Tetrahedra as Molecular Flasks for Selective Reaction Prompting and Luminescent Reaction Tracing. *Chem.—Eur. J.* **2014**, *20*, 2224−2231.
(58) Wu, Z.-L.; Podust, L. M.; Guengerich, F. P. Expansion of substrate specificity of cytochrome P450 2A6 by random and site-directed mutagenesis. *J. Biol. Chem.* **2005**, *280*, 41090−41100.
(59) Guengerich, F. P. Common and uncommon cytochrome P450 reactions related to metabolism and chemical toxicity. *Chem. Res. Toxicol.* **2001**, *14*, 611−650.
(60) De Rienzo, F.; Fanelli, F.; Menziani, M. C.; De Benedetti, P. G. Theoretical investigation of substrate specificity for cytochromes P450 IA2, P450 IID6 and P450 IIIA4. *J. Comput. Aided Mol. Des.* **2000**, *14*, 93−116.
(61) Behrendorff, J. B. Y. H.; Huang, W.; Gillam, E. M. Directed evolution of cytochrome P450 enzymes for biocatalysis: exploiting the catalytic versatility of enzymes with relaxed substrate specificity. *Biochem. J.* **2015**, *467*, 1−15.

https://doi.org/10.1021/jacsau.4c00539
JACS Au 2024, 4, 3238−3247

(62) Brazier-Hicks, M.; Franco-Ortega, S.; Watson, P.; Rougemont, B.; Cohn, J.; Dale, R.; Hawkes, T. R.; Goldberg-Cavalleri, A.; Onkokesung, N.; Edwards, R. Characterization of cytochrome P450s with key roles in determining herbicide selectivity in maize. *ACS Omega* **2022**, *7*, 17416−17431.
(63) Jing, L.-P.; Sun, J.-S.; Sun, F.; Chen, P.; Zhu, G. Porous aromatic framework with mesopores as a platform for a super-efficient heterogeneous Pd-based organometallic catalysis. *Chem. Sci.* **2018**, *9*, 3523−3530.
(64) Riscoe, A. R.; Wrasman, C. J.; Menon, A.; Dinakar, B.; Goodman, E. D.; Kunz, L. Y.; Yacob, S.; Cargnello, M. Chemically Controllable Porous Polymer−Nanocrystal Composites with Hierarchical Arrangement Show Substrate Transport Selectivity. *Chem. Mater.* **2020**, *32*, 5904−5915.
(65) Lan, S.; Ling, L.; Wang, S.; Ma, D. Pillar [5] arene-integrated three-dimensional framework polymers for macrocycle-induced size-selective catalysis. *ACS Appl. Mater. Interfaces* **2022**, *14*, 4197−4203.
(66) He, H.; Xue, Y.-Q.; Wang, S.-Q.; Zhu, Q.-Q.; Chen, J.; Li, C.-P.; Du, M. A double-walled bimetal−organic framework for antibiotics sensing and size-selective catalysis. *Inorg. Chem.* **2018**, *57*, 15062−15068.
(67) Yang, L.; Cai, P.; Zhang, L.; Xu, X.; Yakovenko, A. A.; Wang, Q.; Pang, J.; Yuan, S.; Zou, X.; Huang, N.; et al. Ligand-directed conformational control over porphyrinic zirconium metal−organic frameworks for size-selective catalysis. *J. Am. Chem. Soc.* **2021**, *143*, 12129−12137.
(68) Fang, Q.-R.; Yuan, D.-Q.; Sculley, J.; Li, J.-R.; Han, Z.-B.; Zhou, H.-C. Functional mesoporous metal− organic frameworks for the capture of heavy metal ions and size-selective catalysis. *Inorg. Chem.* **2010**, *49*, 11637−11642.
(69) Yang, Y.; Wang, F.; Yang, Q.; Hu, Y.; Yan, H.; Chen, Y.-Z.; Liu, H.; Zhang, G.; Lu, J.; Jiang, H.-L.; et al. Hollow metal−organic framework nanospheres via emulsion-based interfacial synthesis and their application in size-selective catalysis. *ACS Appl. Mater. Interfaces* **2014**, *6*, 18163−18171.
(70) Wu, S. M.; Yang, X. Y.; Janiak, C. Confinement effects in zeolite-confined noble metals. *Angew. Chem., Int. Ed.* **2019**, *58*, 12340−12354.
(71) Laursen, A. B.; Højholt, K. T.; Lundegaard, L. F.; Simonsen, S. B.; Helveg, S.; Schüth, F.; Paul, M.; Grunwaldt, J. D.; Kegnæs, S.; Christensen, C. H.; et al. Substrate size-selective catalysis with zeolite-encapsulated gold nanoparticles. *Angew. Chem., Int. Ed.* **2010**, *49*, 3504−3507.
(72) Liu, L.; Díaz, U.; Arenal, R.; Agostini, G.; Concepción, P.; Corma, A. Erratum: Generation of subnanometric platinum with high stability during transformation of a 2D zeolite into 3D. *Nat. Mater.* **2017**, *16*, 597.
(73) Fang, Q.; Gu, S.; Zheng, J.; Zhuang, Z.; Qiu, S.; Yan, Y. 3D microporous base-functionalized covalent organic frameworks for size-selective catalysis. *Angew. Chem., Int. Ed.* **2014**, *53*, 2878−2882.
(74) Meng, Y.; Luo, Y.; Shi, J. L.; Ding, H.; Lang, X.; Chen, W.; Zheng, A.; Sun, J.; Wang, C. 2D and 3D porphyrinic covalent organic frameworks: the influence of dimensionality on functionality. *Angew. Chem., Int. Ed.* **2020**, *59*, 3624−3629.
(75) Shi, Y.; Zhang, X.; Liu, H.; Han, J.; Yang, Z.; Gu, L.; Tang, Z. Metalation of catechol-functionalized defective covalent organic frameworks for lewis acid catalysis. *Small* **2020**, *16*, 2001998.
(76) Otte, M.; Kuijpers, P. F.; Troeppner, O.; Ivanović-Burmazović, I.; Reek, J. N.; de Bruin, B. Encapsulated Cobalt−Porphyrin as a Catalyst for Size-Selective Radical-type Cyclopropanation Reactions. *Chem.—Eur. J.* **2014**, *20*, 4880−4884.
(77) Leung, D. H.; Bergman, R. G.; Raymond, K. N. Highly selective supramolecular catalyzed allylic alcohol isomerization. *J. Am. Chem. Soc.* **2007**, *129*, 2746−2747.
(78) Ziegler-Skylakakis, K.; Fabri, J.; Graeser, U.; Simo, T. A. Xylenes. *Ullmann's Encyclopedia of Industrial Chemistry*; Wiley, 2019; pp 1−20.
(79) de Almeida, J. L. G.; Dufaux, M.; Taarit, Y. B.; Naccache, C. Linear alkylbenzene. *J. Am. Oil Chem. Soc.* **1994**, *71*, 675−694.
(80) Mal, D. D.; Khilari, S.; Pradhan, D. Efficient and selective oxidation of toluene to benzaldehyde on manganese tungstate nanobars: a noble metal-free approach. *Green Chem.* **2018**, *20*, 2279−2289.
(81) Ye, Z.; Giraudon, J.-M.; Nuns, N.; Simon, P.; De Geyter, N.; Morent, R.; Lamonier, J.-F. Influence of the preparation method on the activity of copper-manganese oxides for toluene total oxidation. *Appl. Catal., B* **2018**, *223*, 154−166.
(82) Bertolini, G. R.; Pizzio, L. R.; Kubacka, A.; Muñoz-Batista, M. J.; Fernández-García, M. Composite H3PW12O40−TiO2 catalysts for toluene selective photo-oxidation. *Appl. Catal., B* **2018**, *225*, 100−109.
(83) Merkushev, E. Advances in the synthesis of iodoaromatic compounds. *Synthesis* **1988**, *1988*, 923−937.
(84) Mo, J.; Zhang, Y.; Xu, Q.; Zhu, Y.; Lamson, J. J.; Zhao, R. Determination and risk assessment of by-products resulting from photocatalytic oxidation of toluene. *Appl. Catal., B* **2009**, *89*, 570−576.
(85) Kuljiraseth, J.; Wangriya, A.; Malones, J.; Klysubun, W.; Jitkarnka, S. Synthesis and characterization of AMO LDH-derived mixed oxides with various Mg/Al ratios as acid−basic catalysts for esterification of benzoic acid with 2-ethylhexanol. *Appl. Catal., B* **2019**, *243*, 415−427.
(86) Giri, R.; Yu, J.-Q. Synthesis of 1, 2-and 1, 3-dicarboxylic acids via Pd (II)-catalyzed carboxylation of aryl and vinyl C− H bonds. *J. Am. Chem. Soc.* **2008**, *130*, 14082−14083.
(87) Connolly, T. J.; Matchett, M.; McGarry, P.; Sukhtankar, S.; Zhu, J. A practical synthesis of 3, 4-dimethoxy-o-toluic acid. *Org. Process Res. Dev.* **2004**, *8*, 624−627.
(88) Saha, R.; Sekar, G. Selective oxidation of alkylarenes to aromatic acids/ketone in water by using reusable binaphthyl stabilized Pt nanoparticles (Pt-BNP) as catalyst. *Appl. Catal., B* **2019**, *250*, 325−336.
(89) Song, G.; Feng, L.; Xu, J.; Zhu, H. Liquid-phase oxidation of toluene to benzaldehyde with molecular oxygen catalyzed by copper nanoparticles supported on graphene. *Res. Chem. Intermed.* **2018**, *44*, 4989−4998.
(90) Nakai, T.; Iwai, T.; Mihara, M.; Ito, T.; Mizuno, T. Novel oxidation of toluenes catalyzed by reusable vanadyl (IV) sulfate under mild conditions with molecular oxygen. *Tetrahedron Lett.* **2010**, *51*, 2225−2227.
(91) Hirai, N.; Sawatari, N.; Nakamura, N.; Sakaguchi, S.; Ishii, Y. Oxidation of Substituted Toluenes with Molecular Oxygen in the Presence of N,N',N"-Trihydroxyisocyanuric Acid as a Key Catalyst. *J. Org. Chem.* **2003**, *68*, 6587−6590.
(92) Ilyas, M.; Sadiq, M. Oxidation of toluene to benzoic acid catalyzed by platinum supported on zirconia in the liquid phase-solvent free conditions. *Catal. Lett.* **2009**, *128*, 337−342.
(93) Kesavan, L.; Tiruvalam, R.; Rahim, M. H. A.; bin Saiman, M. I.; Enache, D. I.; Jenkins, R. L.; Dimitratos, N.; Lopez-Sanchez, J. A.; Taylor, S. H.; Knight, D. W.; et al. Solvent-free oxidation of primary carbon-hydrogen bonds in toluene using Au-Pd alloy nanoparticles. *Science* **2011**, *331*, 195−199.
(94) Brutchey, R. L.; Drake, I. J.; Bell, A. T.; Tilley, T. D. Liquid-phase oxidation of alkylaromatics by a H-atom transfer mechanism with a new heterogeneous CoSBA-15 catalyst. *Chem. Commun.* **2005**, 3736−3738.
(95) Wang, F.; Xu, J.; Li, X.; Gao, J.; Zhou, L.; Ohnishi, R. Liquid phase oxidation of toluene to benzaldehyde with molecular oxygen over copper-based heterogeneous catalysts. *Adv. Synth. Catal.* **2005**, *347*, 1987−1992.
(96) Polshettiwar, V.; Varma, R. S. Green chemistry by nano-catalysis. *Green Chem.* **2010**, *12*, 743−754.
(97) Polshettiwar, V.; Luque, R.; Fihri, A.; Zhu, H.; Bouhrara, M.; Basset, J.-M. Magnetically recoverable nanocatalysts. *Chem. Rev.* **2011**, *111*, 3036−3075.
(98) Liu, B.; Romine, A. M.; Rubel, C. Z.; Engle, K. M.; Shi, B.-F. Transition-metal-catalyzed, coordination-assisted functionalization of

https://doi.org/10.1021/jacsau.4c00539
JACS Au 2024, 4, 3238−3247

nonactivated C (sp3)−H bonds. *Chem. Rev.* **2021**, *121*, 14957−15074.
(99) Holmberg-Douglas, N.; Nicewicz, D. A. Photoredox-catalyzed C−H functionalization reactions. *Chem. Rev.* **2022**, *122*, 1925−2016.
(100) Gutekunst, W. R.; Baran, P. S. C−H functionalization logic in total synthesis. *Chem. Soc. Rev.* **2011**, *40*, 1976−1991.
(101) Shilov, A. E.; Shul'pin, G. B. Activation of C− H bonds by metal complexes. *Chem. Rev.* **1997**, *97*, 2879−2932.
(102) Vallavoju, N.; Sivaguru, J. Supramolecular photocatalysis: combining confinement and non-covalent interactions to control light initiated reactions. *Chem. Soc. Rev.* **2014**, *43*, 4084−4101.
(103) Gera, R.; Das, A.; Jha, A.; Dasgupta, J. Light-induced proton-coupled electron transfer inside a nanocage. *J. Am. Chem. Soc.* **2014**, *136*, 15909−15912.
(104) Das, A.; Mandal, I.; Venkatramani, R.; Dasgupta, J. Ultrafast photoactivation of C− H bonds inside water-soluble nanocages. *Sci. Adv.* **2019**, *5*, No. eaav4806.
(105) Lü, J.; Han, L.-W.; Alsmail, N. H.; Blake, A. J.; Lewis, W.; Cao, R.; Schröder, M. Control of assembly of dihydropyridyl and pyridyl molecules via directed hydrogen bonding. *Cryst. Growth Des.* **2015**, *15*, 4219−4224.
(106) Lü, J.; Perez-Krap, C.; Suyetin, M.; Alsmail, N. H.; Yan, Y.; Yang, S.; Lewis, W.; Bichoutskaia, E.; Tang, C. C.; Blake, A. J.; et al. A robust binary supramolecular organic framework (SOF) with high CO2 adsorption and selectivity. *J. Am. Chem. Soc.* **2014**, *136*, 12828−12831.
(107) Yang, W.; Greenaway, A.; Lin, X.; Matsuda, R.; Blake, A. J.; Wilson, C.; Lewis, W.; Hubberstey, P.; Kitagawa, S.; Champness, N. R.; et al. Exceptional thermal stability in a supramolecular organic framework: porosity and gas storage. *J. Am. Chem. Soc.* **2010**, *132*, 14457−14469.
(108) Deposition number 2268668 (for MC) contains the supplementary crystallographic data for this paper. This data is provided free of charge by the joint Cambridge Crystallographic Data Centre.
(109) Maglic, J. B.; Lavendomme, R. MoloVol: an easy-to-use program for analyzing cavities, volumes and surface areas of chemical structures. *J. Appl. Crystallogr.* **2022**, *55*, 1033−1044.
(110) Thordarson, P. Determining association constants from titration experiments in supramolecular chemistry. *Chem. Soc. Rev.* **2011**, *40*, 1305−1323.
(111) Stewart, J. J. Optimization of parameters for semiempirical methods V: Modification of NDDO approximations and application to 70 elements. *J. Mol. Model.* **2007**, *13*, 1173−1213.
(112) Roy, D.; Paul, S.; Dasgupta, J. Visible light-mediated C (sp 3)−H bond functionalization inside an all-organic nanocavity. *Chem. Commun.* **2023**, *59*, 13143−13146.
(113) Ghosal, S.; Das, A.; Roy, D.; Dasgupta, J. Tuning light-driven oxidation of styrene inside water-soluble nanocages. *Nat. Commun.* **2024**, *15*, 1810.
(114) Rehm, D.; Weller, A. Kinetics of fluorescence quenching by electron and H-atom transfer. *Isr. J. Chem.* **1970**, *8*, 259−271.
(115) Arman Taherpour, A. Theoretical studies of the free energies of electron transfer and electron transfer kinetics in nanostructure supramolecular complexes of cis-unsaturated thiocrown ethers and Ce and Gd endohedral metallofullerenes [X−UT−Y] [M@ C82](M= Ce, Gd). *Arab. J. Chem.* **2017**, *10*, S609−S616.

https://doi.org/10.1021/jacsau.4c00539
JACS Au 2024, 4, 3238−3247